Experimental Characterization of Active Joint for Trunk Exoskeleton

Experimental Characterization of Active Joint for Trunk Exoskeleton

Mattia Antonelli[1], Elisa Panero[1], Michele Polito[1], Laura Gastaldi[1], Stefano Pastorelli[1]

[1] Dept. of Mechanical and Aerospace Engineering, Politecnico di Torino, Turin, Italy
mattia.antonelli@polito.it

Abstract. Wearable robotics is one of the Industry 4.0 pillars for performing tasks that cannot yet be fully automated. This category includes trunk exoskeletons, devices that can be worn directly by the user with the aim of partially reducing low-back muscular efforts and avoiding work-related injuries. Active exoskeletons allow a good support adaptability to suit user's request, certifying the relevance of a control law able to modulate the assistance also compensating the disturbances. The aim of this study is to experimentally characterize active joints of a trunk exoskeleton prototype to obtain a model able to describe their real behaviour and non-linearities. This identification is essential to develop an adaptable and disturbance-free control law that ensures the flexible desired support.

Keywords: Wearable robotics, Trunk-support exoskeleton, Human-robot inter-face, Mechanical modelling, Industry.

1 Introduction

Collaborative robotics represents a cutting edge solution, with robots and humans coexisting in the same workspace [1]. Collaborative robotics includes also systems in direct contact with the user, namely wearable technologies [2, 3]. Exoskeletons fall in this category. They might support workers by reducing physical effort during repetitive and fatiguing tasks [4, 5] and ensure ergonomic and safety conditions. Indeed, weight manual handling, maintaining static posture and lifting external objects expose operators to work-related musculoskeletal disorders (WMSDs), especially if they are repetitive or prolonged in time [6]. In particular, the most frequent WMSD among workers is low back pain [7]. In this context, back exoskeletons are a promising solution to assist and support workers during specific task reducing human physical efforts. Both passive and active exoskeletons had been considered [8, 9].
Despite passive actuation being cheaper, lightweight and less complex, active systems allow to achieve high flexibility and to ensure more and customizable applications [10]. Hence, it is necessary to design a control strategy that takes full advantage of the active exoskeletons versatility to enhance the potential impact in the industrial scenario [11].

The aim of this study is the mechanical characterization of active joints designed for a trunk exoskeleton [12], the development of a numerical model and its experimental validation.

2 System description

A scheme of the trunk exoskeleton is reported in Fig. 1a, where the right side is depicted. It consists in a rigid segment to support the trunk (*trunk support*), a second rigid element at the level of the thigh (*leg support*) and an adaptable *pelvis belt*. The active joint is positioned coaxially with respect to the user's hip and it is composed of two coaxial hinges that connect the pelvis belt with the thigh support and the thigh support with the trunk support, respectively. The human-exoskeleton interfaces at trunk and thigh allow vertical translation, while rotation in sagittal plane is allowed by the joint. The assistance torque provided by the active joint acts between the *trunk support* and the *leg support*, with the aim to reduce joint load and spine muscles effort during torso flexion/extension.

2.1 Joint Design

The active joint structure is illustrated in Fig. 1b. Each joint comprises a gearmotor system consisting of an *electric motor* coupled with a harmonic reducer (Harmonic Drive HD), for the purpose of ensuring limited dimensions and weight. The motor and the harmonic reducer are connected by the Motor Flange. The Flex Spline element of the HD is coupled with the leg flange, which is integral with the *leg support*. Similarly, the Circular Spline element of the HD is coupled to the trunk flange, which is integral with the *trunk support*. The Wave Generator is directly mounted on the motor shaft.

Two brushless EC60 flat DC motors (Maxon ®, Switzerland), with a nominal torque of 401 mNm, and two CPU-20A-160 Harmonic Drive (HD) reducers (Harmonic Drive AG, Germany) with a reduction ratio of 160, were chosen. Sensors measuring actual angular position, velocity and current are embedded in the Maxon motors. The mass of a joint unit is 2,3 kg while the one of the wearable device is 6,5 kg; however the prototype has not been optimized in weight yet.

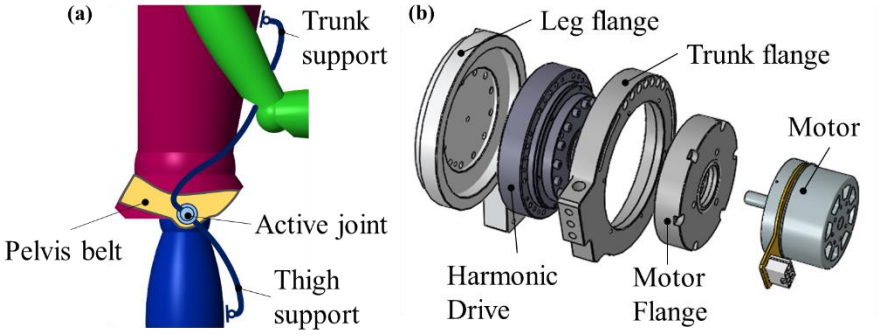

Fig. 1. Active exoskeleton prototype (a) and the right joint components (b) [12].

A two-level control strategy is adopted. The high-level control imposes the desired torque to the device, instead the low-level control consists in the direct manage of the actuators in a closed-loop control. The human motion is described by the angular

displacement between human body parts (trunk, pelvis, thighs) and thus two encoders, one integrated within the motor and an external one, measure the angles between trunk and thighs and between thighs and pelvis respectively. Starting from the kinematic information, the joint high-level control strategy generates a torque set for the actuators, modulating the assistance appropriately.

The HD has several strengths compared to other reduction systems, including high precision, compactness and lightness. Moreover, also with high transmission ratios, the HD keeps a noticeable efficiency. However, despite many advantages, it may introduce undesired issues such as a non-linear friction. For this reason, the characterization of the system becomes crucial, for the further assessment of the transmission effectiveness. Once the real dynamic response of the active joints is identified, the torque control can be set, suiting the user's needs.

2.2 Experimental test bench

The EC60 flat DC motors were managed by two drivers EPOS4 50/15 CAN (Maxon ®, Switzerland) linked to a PC, used as the control master node, through a CAN interface (NI CAN USB-8502, National Instruments ®, USA). In this first prototype, only the actuation system and the sensors were integrated into the joints, while the master control unit and the powering system were remote.

Labview (National Instruments ®, USA) was used as development environment for the implementation of the high-level control scheme and to set the reference torque.

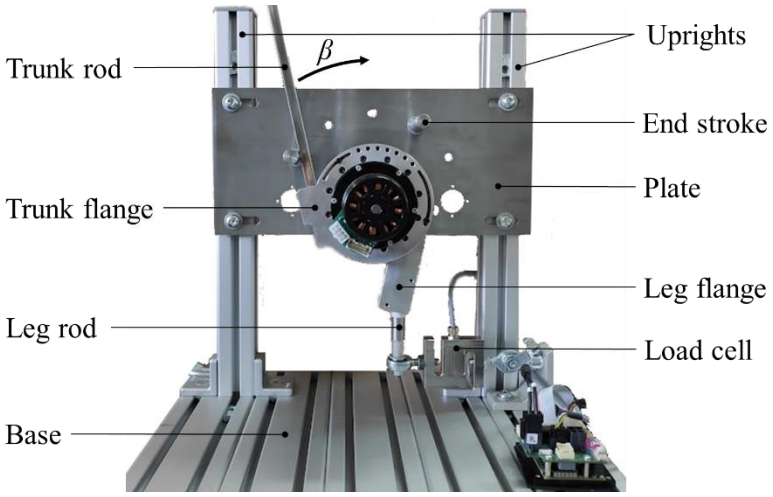

Fig. 2. Test bench and right joint components.

To assess the joint transmission system, a test bench was set up (Fig. 2). The test bench consists of a base, two vertical uprights fixed to it and a rectangular steel plate, mounted on the uprights. The active joint was fixed on the plate, in particular the leg flange was mounted on the plate by means of a Teflon bushing to allow friction-free

rotation with respect to the plate. A cylindrical element (*leg rod*) was fixed on the lower part of the leg flange. The lower end of the *leg rod* is connected to a load cell (ME-Meßsysteme ®, Germany, KD80S, full scale 500 N), which is clamped to the base. A *trunk rod* was inserted in the trunk flange to extend it for an easier handling. The angular displacement β of the trunk flange is measured with respect to the *trunk rod* initial position, as shown in Fig. 2. Five equally spaced holes on the plate accommodated pegs that can act as reference angle or end strokes.

When applying a force F_t to the *trunk rod* (simulating the force exerted by the user's chest), the load cell measures the force F_c transmitted by the joint to the *leg rod* (simulating the force exchanged at user's thighs) as depicted in Fig. 3. Left and right joints were tested separately.

3 Characterization of the system

3.1 Joint model

The joint model is evaluated through the free body diagram of its components (Fig. 3).

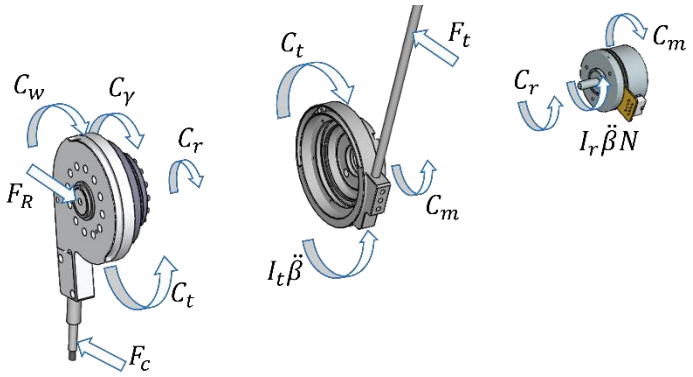

Fig. 3. Free body diagram of the right joint mounted on the test bench.

The summing-up equilibrium equations of the system are:

$$F_t l_t + C_m + I_t\ddot{\beta} = C_t \tag{1}$$

$$F_c l_c = C_m(N-1) - I_a\ddot{\beta} - C_\beta - C_0 - C_w \tag{2}$$

Where $\ddot{\beta}$ is the trunk flange angular acceleration and N is the transmission ratio. F_t is the force applied to the *trunk rod* and F_c the load cell force applied at distance l_t and l_c from the joint axis respectively; F_R is the reaction force. C_m is the motor torque; C_r and C_t the HD input and output torques respectively; C_w the torque due to the unbalanced system weight; C_γ the total equivalent dissipative torque at the trunk axis (sum of the viscous torque C_β and a constant torque offset C_0). I_t and I_r are the moments of inertia of the trunk part and motor rotor; I_a is the apparent motor moment of inertia at the trunk axis.

3.2 Characterization of viscous friction within the joint

The viscous friction C_β within the active joint was considered. The motor was speed controlled, with a trapezoidal reference and one turn back and forth of the joint. Different maximum angular velocities were set (5, 10, 20, 30, 40, 50, 60, 70, 80 and 90 deg/s) and ten trials were conducted for each speed. In correspondence of the constant velocity interval, the current absorbed by the motor was considered. These values of current are directly proportional to the motor torque necessary to maintain a constant speed. The Curve Fitting Tool (MATLAB ®, MathWorks, USA) was utilized starting from the experimental data collected, with the aim of obtaining the viscous torque as a function of the trunk flange velocity $\dot{\beta}$.

Since the absolute values of the torque assessed with positive and negative speeds were comparable, they were averaged. The function that fitted best the experimental data, as can be seen in Fig. 4a, was a second-degree polynomial (3) configured with the "Bisquare" method, with a confidence interval of 95%, where the coefficient *a*, *b* and *c* are summarized in Table 1 for both the joints.

$$C_\beta = a\,\dot{\beta}^2 sign(\dot{\beta}) + b\,\dot{\beta} + c\,sign(\dot{\beta}) \tag{3}$$

3.3 Characterization of the weight effect

Due to the asymmetry of the joint, the centre of rotation did not match the centre of gravity, therefore a torque due to the weight force was present. The effect of the weight force was experimentally assessed by considering the product between the forces sensed by the load cell, for different positions of the *trunk rod*, and the distance l_c. The angle β, was varied from the zero-reference angle, increasing it with steps of 10°, up to the angle 116,5°, which is the maximum angle position allowed by the constrains.

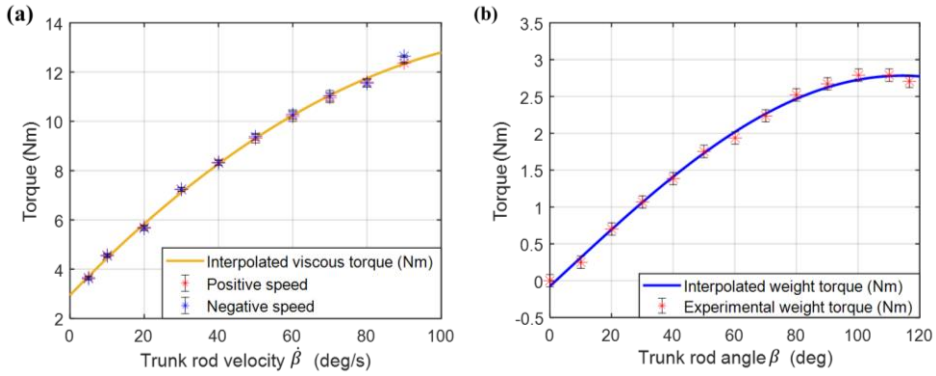

Fig. 4. Experimental interpolation of (a) viscous torque and (b) weight torque for the right joint.

Using the obtained experimental data, it was possible to fit a function (Fig. 4b) describing the relationship between the angle covered and the weight torque C_w. The best

fitting was achieved with a sinusoidal function (4) and its parameters are reported in Table 1 for both the joints.

$$C_w = C_{w0}\sin(s\beta + \varphi) \tag{4}$$

3.4 Characterization of moment of inertia and torque offset

To evaluate the moment of inertia I_a and torque offset C_0 of equation (2), twenty tests were carried out in which the *trunk rod* was randomly moved by an operator, simulating trunk flexion and extension. During these tests, the motor torque C_m was set to zero and the *trunk rod* angular position β, angular velocity $\dot{\beta}$ and the cell force F_c were recorded. In addition, the acceleration $\ddot{\beta}$ was derived by the velocity after filtering it through a 2Hz low-pass band filter. The viscous torque was calculated from the equation (3) using the recorded velocity and the weight torque was computed according to equation (4).

Starting from these data and relying on the descriptive equation of the system (2), the cost function *fmeansearch* (MATLAB ®) was used to find the optimized parameters for I_a and C_0, in accordance with the equation (5).

$$\sum\left(\left(F_c l_c - C_m(N-1) + C_\beta + C_w\right) - \left(-I_a\ddot{\beta} - C_0\right)\right)^2 = 0 \tag{5}$$

The moment of inertia and offset values found with the fitting are reported in Table 1.

Table 1. Characterization values of viscous torque, weight torque, moment of inertia and offset parameters for both joints.

	a *(Nms²/deg²)*	*b* *(Nms/deg)*	*c* *(Nm)*	C_{w0} *(Nm)*	*s*	φ *(rad)*	I_a *(kgm²)*	C_0 *(Nm)*
Right Joint	$5{,}77\ 10^{-4}$	0,156	2,32	2,79	0,014	-0,027	2,37	-0,59
Left Joint	$6{,}52\ 10^{-4}$	0,164	2,94	2,59	0,013	-3,108	3,21	0,20

3.5 Numerical validation

Five further tests were realized with the aim of validating the characterization parameters. In these new tests, a current reference proportional to the angle β was imposed on the motor, in order to check that the force estimated using the parameters found by the characterization is still similar to the real load cell measure.

The difference between the force estimated through the model and the actual force measured by the load cell was evaluated through the RMSE (Root Mean Square Error) and the Pearson correlation coefficient r^2. For both joints, the RMSE and correlation values were below 1.6 Nm and above 0,98 respectively, for all validation tests. As can be observed in Fig. 5a, during dynamic intervals of the trials the error is lower, while it worsens slightly in static situations. This is assumed to be due to the friction variability.

4 Active Set Generation

Using the numerical model, it is possible to set a motor reference signals that takes into account the real behaviour of the joint, in order to provide the desired torque to the user.

Assuming that this should be described as a function of β and $\dot{\beta}$, the reference motor torque consists of a term which is a function of β and $\dot{\beta}$ and a correction term C_c that includes the disturbing effects.

$$C_m = (f(\beta, \dot{\beta}) + C_c)/(N-1) \tag{6}$$

Therefore:

$$C_c = I_a\ddot{\beta} + C_\beta + C_w + C_0 \tag{7}$$

However, if the joint disturbing effects were fully compensated, the system would be undamped. This would lead to instability and uncomfortable oscillations for the user. One way to avoid such instability is to introduce only a percentage of the correction factor when evaluating to the ideal reference law.

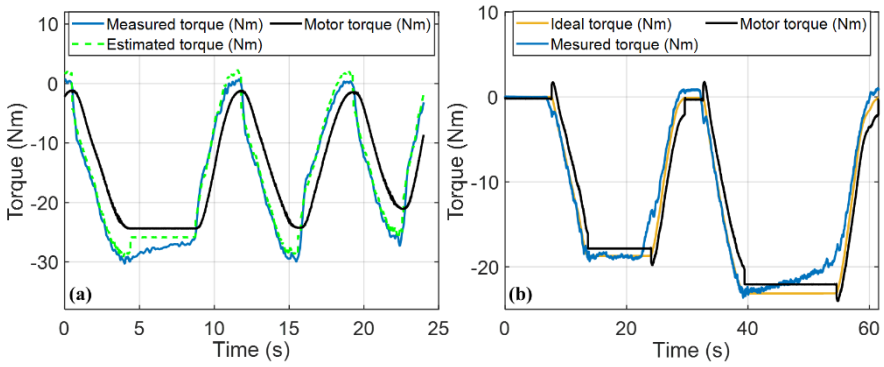

Fig. 5. Comparison between estimated, measured and motor torques in a validation test (a). Ideal, measured and motor torques in a test after the correction (b).

With the goal of checking how the correction of the torque reference affects the response of the real system, ten tests characterized by random rotation movements of the *trunk rod* operated manually were carried out for both the joints. In particular, the ideal support torque was designed as proportional to the angle of the trunk flange β, defining K as the proportional constant. During a preliminary test, the percentage of the correction factor was set equal to 70%, according to operator's perception of system stability. Thus, the torque set imposed to the motor is described by (8):

$$C_m = (K\beta + 0{,}7\ C_c)/(N-1) \tag{8}$$

Fig.5a illustrates a trial example of desired torque, measured torque, and motor reference torque. To evaluate the error between the desired torque and the real one, the RMSE was calculated for each trial and averaged between trials. The right joint RMSE presented a value of 2,04±0,79 Nm, while the left one was equal to 2,51±0,62 Nm.

5 Conclusions

The current study presented the experimental characterization of active joints of a trunk-support exoskeleton prototype for worker's assistance during handling tasks. A test bench was built with the aim of characterising the joints and defining a numerical model. This was exploited to compensate friction and non-linear effects in the joint when setting the reference motor torque.

Experimental data were recorded and RMSE between the experimental torque and the reference one was calculated. RMSE values were lower than the 3% of the maximum torque provided by the motor.

The described model can be considered valid for defining a robust correction for the motor output torque, with the aim of ensuring the ideal support.

6 References

1. Digo, E., Antonelli, M., Cornagliotto, V., Pastorelli, S., Gastaldi, L.: Collection and analysis of human upper limbs motion features for collaborative robotic applications. Robotics. 9,33 (2020).
2. Digo, E., Gastaldi, L., Antonelli, M., Pastorelli, S., Cereatti, A., Caruso, M.: Real-time estimation of upper limbs kinematics with IMUs during typical industrial gestures. In: 3rd International Conference on Industry 4.0 and Smart Manufacturing, 1041-1047 (2022).
3. McDevitt, S., Hernandez, H., Hicks, J., Lowell, R., Bentahaikt, H., Burch, R., Ball, J., Chander, H., Freeman, C., Taylor, C., Anderson, B.: Wearables for Biomechanical Performance Optimization and Risk Assessment in Industrial and Sports Applications. Bioengineering. 9,33 (2022).
4. De Looze, M.P., Bosch, T., Krause, F., Stadler, K.S., O'Sullivan, L.W.: Exoskeletons for industrial application and their potential effects on physical work load. Ergonomics. 59, 671–681 (2016).
5. Toxiri, S., Näf, M.B., Lazzaroni, M., Fernández, J., Sposito, M., Poliero, T., Monica, L., Anastasi, S., Caldwell, D.G., Ortiz, J.: Back-Support Exoskeletons for Occupational Use: An Overview of Technological Advances and Trends, IISE Transactions on Occupational Ergonomics and Human Factors, 7:3-4, 237-249 (2019).
6. The National Institute for Occupational Safety e Health. NIOSH - https://www.cdc.gov/niosh/index.html
7. Kok, J., Vroonhof, P., Snijders, J., Roullis, G., Clarke, M., Peereboom, K., Dorst, P., Isusi, I.: Work-related musculoskeletal disorders : prevalence, costs and demographics in the EU. Publications Office, EU-OSHA (2020).
8. Babič, J., Petrič, T., Mombaur, K., Kingma, I., Bornmann, J., González-Vargas, J., Baltrusch, S., Šarabon, N., Houdijk, H.: SPEXOR: Design and development of passive spinal exoskeletal robot for low back pain prevention and vocational reintegration. SN Appl. Sci. 1, 1–5 (2019).
9. Ji, X., Wang, D., Li, P., Zheng, L., Sun, J., Wu, X.: SIAT-WEXV2: A wearable exoskeleton for reducing lumbar load during lifting tasks. Complexity. 2020, (2020).
10. Ali, A., Fontanari, V., Schmoelz, W., Agrawal, S.K.: Systematic Review of Back-Support Exoskeletons and Soft Robotic Suits. Front. Bioeng. Biotechnol. 9, 1–15 (2021).
11. Toxiri, S., Koopman, A.S., Lazzaroni, M., Ortiz, J., Power, V., de Looze, M.P., O'Sullivan, L., Caldwell, D.G.: Rationale, implementation and evaluation of assistive strategies for an active back-support exoskeleton. Front. Robot. AI. 5, 1–14 (2018).
12. Panero, E., Muscolo, G.G., Gastaldi, L., Pastorelli, S.: Multibody Analysis of a 3D Human Model with Trunk Exoskeleton for Industrial Applications. In: Computational Methods in Applied Sciences. pp. 43–51. Springer (2020).